

## TRANSMISSION ELECTRON MICROSCOPY (TEM) APPLIED TO ANCIENT POTTERY\*

M. P. MATA,<sup>1,2</sup> D. R. PEACOR<sup>1</sup> and M. D. GALLART-MARTÍ<sup>3</sup>

<sup>1</sup>Department of Geological Sciences, The University of Michigan, Ann Arbor, MI 48105-103, USA

<sup>2</sup>Dept. Geología. Fac. Ciencias del Mar, Universidad de Cádiz, 11510 Pto. Real, Cádiz, Spain

<sup>3</sup>Dept. Ciencias de la Tierra, Universidad de Zaragoza, Pedro Cerbuna, 12, 50009 Zaragoza, Spain

*A comparative study of ancient pottery has been carried out, which utilized X-ray diffraction, optics and scanning and transmission electron microscopy (SEM and TEM). Samples came from three prehistoric sites in northern Spain (La Rioja). Transmission electron microscope techniques, which use intact ion-milled samples, allow minerals and glass to be imaged in situ, providing data on textures, crystal structures and composition. TEM provided detailed characterization of both source-characteristic raw materials and products of the firing process, and revealed the range of intermediate phases, most of which had sizes beyond that of resolution by SEM. More importantly, TEM provided definition of the reaction processes, from starting materials through glass and new crystalline phases, providing data on both temperature and duration of firing.*

**KEYWORDS:** ELECTRON MICROSCOPE TECHNIQUES, PREHISTORIC POTTERY, LA RIOJA (SPAIN), TRANSMISSION ELECTRON MICROSCOPY, REACTION PROCESSES, MICROTERTURES

### INTRODUCTION

In studies of ancient pottery, complete characterization of coarse grains and fine-grained matrices is essential for determination of original source minerals, firing temperatures, manufacturing processes and characterization of post-depositional changes. Both chemical and mineralogical methods are used to obtain such information (for recent reviews, see Rice 1987; Velde and Druc 1999, and references therein). X-ray diffraction (XRD), optical microscopy and scanning electron microscopy (SEM) are significant mineralogical techniques. SEM is a particularly powerful method, as secondary- and backscattered-electron SEM imaging (SE-BSE) combined with qualitative energy-dispersive spectroscopic (EDS) analysis provides information about microstructure, degree of vitrification, the nature of inclusions and slips and, to a lesser extent, definition of alteration features, which collectively contribute to the characterization of sample provenance (Tite and Maniatis 1975; Maniatis and Tite 1981; Edwards and Segnit 1984; Freestone and Middleton 1987; Middleton 1987; Tite 1992; Aguarod Otal *et al.* 1995; Fabbri 1996; Klykova *et al.* 1998; Mallory-Greenouh *et al.* 1998). However, these mineralogical techniques do have some disadvantages; for example, XRD provides crystal structure data, but is usually independent of textural relations and may represent an average of heterogeneous material of more than one origin, such as muscovite and illite, both minerals having a range of altered states produced by firing. Even SEM provides relatively low spatial resolution, and is therefore entirely inadequate for studying most clay minerals, which generally have sizes

\* Received 26 January 2001; accepted 20 August 2001.

© University of Oxford, 2002

below resolution by EDS analysis and BSE imaging, but which may comprise the bulk of the fine-grained matrix.

By contrast, transmission electron microscopy (TEM) allows minerals and amorphous materials such as glass to be imaged at magnifications ranging from those of SEM to near-atomic resolution, thus providing detailed information on textures, which in turn define processes of chemical reaction. Crystal structure can be determined by means of electron diffraction patterns on selected areas (SAED) that can be chosen on the basis of image characteristics. Composition can be determined by analytical electron microscopy (AEM) using EDS systems, resulting in chemical analyses on areas smaller than 20 nm. Moreover, such analyses are quantitatively accurate, in contrast to SEM analyses, which generally provide only qualitative chemical data. Thus, textures, crystal structures and quantitative compositions can all be directly determined on the same specific domains. For example, closely related clay minerals such as smectite (var. montmorillonite), mixed-layered illite–smectite (I/S), illite and muscovite, which occur in nanometer-scale grains in the fine-grained matrix of pottery, can be easily differentiated. More importantly, the processes of change in each of those minerals which are caused by firing can be directly resolved in individual grains.

Because of these characteristics, TEM studies have been especially useful in the study of natural ultra-fine-grained rocks such as mudstones, shales and slates and their constituent clay minerals (Merriman and Peacor 1999, and references therein; Peacor 1992). Detailed textural, compositional and crystal structural data for mineral assemblages define the extent of reactions between coexisting minerals, and define the specific reaction processes. Such relations depend on both the temperature and the duration of reaction, as demonstrated for naturally ‘fired’ rocks that have been subjected to high temperatures for relatively short periods of times, a process called pyrometamorphism (Brearley 1987; Worden *et al.* 1987; Clark and Peacor 1992). Those relations are therefore especially significant for determining characteristics of source materials, temperatures and durations of firing, or the kind and degree of post-burial alteration of ceramic materials.

TEM has occasionally been applied in archaeometric studies. Kingery and Vandiver (1986) showed that the lustre decoration on 13th-century Islamic ware is associated with a high concentration of nanometric silver particles in a thin surface layer in the glaze. Barber and Freestone (1990) applied this technique to study the characteristic of the phases responsible for the dichroic properties of the glass of the Lycurgus Cup, and Pérez-Arantegui *et al.* (2000) studied the glaze and lustre decoration in Renaissance pottery from Gubbio and Deruta (Italy). Nevertheless, TEM has not been applied to studies of ancient pottery.

To illustrate the power of TEM techniques, especially relative to more commonly used methods, we have carried out a study of ceramic materials from three prehistoric sites in northern Spain (La Rioja), using XRD, optical microscopy, SEM and TEM, but with an emphasis on TEM. This study was designed to show how TEM provides insights into the following relations:

- (i) Characterization of original mineral assemblages, with special reference to clay minerals. These data illustrate how completely such minerals can be characterized with respect to textures, compositions and structures, and illustrate how such data can limit provenance.
- (ii) Firing conditions. The TEM data illustrate how, in a single sample, the processes of alteration during firing can be characterized over the complete range from original source materials to maximum alteration. The data show that materials that appear to be homogeneous as studied by other methods provide detailed information on reaction processes. Such data can be related directly to firing temperatures, temperature gradients and firing duration. The data of this study emphasize these specific relations.

(iii) Physical properties. TEM data illustrate how the texture of the fine-grained clay matrix changes with firing temperature, and thus causes structural coherency of the product. This is especially important in prehistoric pottery, for which firing temperatures can be low (<600°C).  
(iv) Post-depositional alteration. TEM has been shown to be a powerful tool in the study of weathering in natural rocks (see, e.g., Banfield and Eggleton 1988, 1990; Hochella and Banfield 1995), which suggests another potential area of application of TEM: alteration of ancient artefacts and stone decay. Characterization of texture, composition and structure permit even subtle changes to be characterized, as illustrated, for example, by the formation of iron oxy-hydroxides in the materials of this study.

Although the results of this study focus on high-resolution characterization of pottery from a single locality, they illustrate the range of capabilities of TEM, which may be used to characterize a variety of archaeological materials, including, for example, materials such as glazes, and coatings as slips responsible for properties such as colour, lustre and so on (see Tite *et al.* 1998, and references therein). Such data lead directly to the goal of defining production technologies, understanding ancient metallurgy and determining the general pattern of development of ceramic technology. TEM has caused a quantum shift in our knowledge of fine-grained geological materials, and has similar potential for much archaeological material.

#### CASE STUDY

Samples for this study came from three prehistoric sites in northern Spain (La Rioja): Bell Beaker and incised–impressed pottery from megalithic sites from Peña Guerra (Nalda, La Rioja) and Collado Palomero (Viguera, La Rioja) (López de Calle and Ilarraz 1997), and from the Bronze Age – Iron Age settlement of Partelapeña (El Redal, La Rioja) (Álvarez Clavijo and Pérez Arrondo 1988). Archaeological levels corresponding to samples PG-1 and PG-4 were dated by the <sup>14</sup>C method to 1500 BC and 1460 ± 60 BC, respectively. Sample Part-15 corresponds to a sherd found in archaeological level III. <sup>14</sup>C radiometric dating yielded an age of 680 ± 50 BC. Sample Part-9 came from lower level I and Part-25 from upper level IV.

Eight ceramic samples were selected from a set of 52 samples previously studied by XRD and optical microscopy. Granulometric and morphometric studies were carried out by means of the digital processing of optical micrographs, by Gallart-Martí and Mata (1995). Table 1 lists characteristics of the samples, the mineral assemblages as determined by XRD and optical microscopy, and the estimated firing temperatures deduced from the mineralogical assemblages by Gallart-Martí and Mata (1995).

#### METHODS

Because TEM observations are obtained on very small volumes, samples must be carefully chosen to represent the desired features, especially in heterogeneous materials. Samples are therefore first studied by low-resolution techniques such as optical microscopy and SEM to obtain an overview of relations. We therefore generally study, by optical microscopy and SEM, the same thin sections that are to be used as a source of TEM samples, and obtain powder XRD patterns to aid in characterizing bulk material. In this case, XRD and optical data were already available. A preliminary SEM study was therefore carried out with secondary electron (SE) and backscattered electron (BSE) images. SE imaging was performed on gold-coated fragments to observe microtextures and the degree of vitrification. SE imaging is sensitive to surface topology, and is therefore generally used to analyse uncut and unpolished samples. BSE

Table 1 *A description of the samples*

<i>Sample</i>	<i>Site</i>	<i>Decoration</i>	<i>Surface treatment</i>	<i>Ca</i>	<i>Q</i>	<i>Int</i>	<i>Ill</i>	<i>Pl</i>	<i>Fd</i>	<i>Do</i>	<i>Di</i>	<i>T (°C)</i>
PG-1	Peña Guerra I	Incised Bell Beaker	Burnished	–	39	51	–	<5	<5	<5	–	650
PG-2	Peña Guerra	Incised, impressed Bell Beaker	Damaged	–	42	54	–	–	<5	–	t	800
PG-4	Peña Guerra	Incised, impressed Bell Beaker	Burnished	10	32	58	–	–	–	–	–	700–750
PG-6	Peña Guerra	Incised Bell Beaker	Damaged	–	54	42	–	–	<5	–	t	800
CP-11	Collado Palomero I	Incised, impressed	Damaged	9	43	–	44	<5	<5	–	–	750
Part-9	Partelapeña (Level I)	Undecorated	Smoothed	47	17	–	32	<5	<5	–	–	450
Part-15	Partelapeña (Level III)	Undecorated	Burnished	5	57	–	38	–	–	–	–	700
Part-25	Partelapeña (Level IV)	Undecorated	Smoothed	22	43	–	28	<5	<5	–	–	700

Ca, calcite; Q, quartz; Int, interstratified illite/smectite; Ill, illite; Pl, plagioclase; Fd, feldspar; Do, dolomite; Di, diopside; t, traces.

images were obtained for both carbon-coated, polished thin sections and portions of thin sections that were further thinned for later TEM observations by bombardment with Ar ions in an ion-mill. BSE images are insensitive to variations in topography, but display levels of greyness that are proportional to the average atomic number of the mineral imaged; for example, they are sensitive to variations in chemical composition. Areas of a polished sample that are found to display a level of greyness can then be analysed by EDS, thus establishing the qualitative composition. We used a Hitachi S-3200N SEM, equipped with a Noran X-ray EDS system, housed in the Electron Microbeam Analysis Laboratory (EMAL) at the University of Michigan.

Following XRD analysis, optical and SE observations, three specimens with firing temperatures estimated to range from  $\sim 450^{\circ}\text{C}$  to  $\sim 850^{\circ}\text{C}$  were selected for TEM study. TEM observations and AEM analyses were obtained with a Philips CM12 scanning-transmission electron microscope (STEM) in the University of Michigan EMAL. It was operated at an accelerating voltage of 120 kV and a beam current of  $\sim 10 \mu\text{A}$ . Samples were prepared by attaching a 3 mm diameter Al washer to the area of a thin section of interest. The washers and attached thin-section areas were removed from the glass-slide backings of the thin sections by gently heating and melting the wax. The samples were then ion-milled and carbon-coated. These procedures were designed to preserve original textures and to permit observation of (001) lattice-fringe images of lattice planes of clay minerals, which were parallel to the electron beam ( $c^*$  perpendicular to the beam). Such fringes correspond directly to individual layers of clay-mineral structures. Lattice-fringe images were obtained at  $75\,000\times$ – $100\,000\times$  magnification, generally using over-focus (100 nm) conditions to maximize the contrast related to compositional differences between adjacent lattice fringes (Veblen *et al.* 1990). A camera length of 770 mm and a selected-area aperture of  $10 \mu\text{m}$  were used to obtain SAED patterns. EDS data were obtained in scanning transmission mode using a Kevex EDS system. A raster of  $200 \text{ nm} \times 200 \text{ nm}$  in scanning mode was used to minimize alkali diffusion and volatilization. Ion-milled standards of paragonite, muscovite, albite, clinocllore, fayalite, rhodonite and titanite were used in the thin-film approximation (Lorimer and Cliff 1976) for quantitative analyses of elements Na, Mg, Al, Si, K, Ca, Ti, Mn and Fe from X-ray energy-dispersive spectra, using  $k$ -factors as defined by Jiang *et al.* (1990). AEM analyses were obtained only from grains that were first characterized by TEM imaging and SAED patterns. Clay minerals were imaged and characterized using the techniques of Guthrie and Veblen (1989, 1990), Veblen *et al.* (1990) and Jiang *et al.* (1990). Mineral identification was based on collective data on textures, spacings of lattice fringes, SAED patterns and AEM analyses.

## RESULTS

### *Scanning electron microscopy (SEM)*

Samples Part-9 and PG-1, which are Ca-rich and Ca-poor, respectively, are representative of low-temperature firing conditions ( $<650^{\circ}\text{C}$ ). SE and BSE images of untreated fragments show similar microtextures. Abundant coarse grains of calcite, (sample Part-9), quartz, K-feldspar (sample Pg-1) and phyllosilicates can be seen immersed in a fine-grained matrix (Figs 1 (A) and (B)). Calcite grains have characteristic rhombohedral cleavage (Figs 1 (A) and (C)), a wide range of sizes up to 0.5 mm and sharp contacts with the matrix, whereas quartz and K-feldspar show rounded shapes. EDS analyses of mica indicate a muscovite-like composition, but the composition is variable, as indicated by brighter cores and darker rims in the BSE images (Fig. 1 (D)). That is consistent with a higher proportion of Fe in the cores. EDS analyses of homogeneous areas

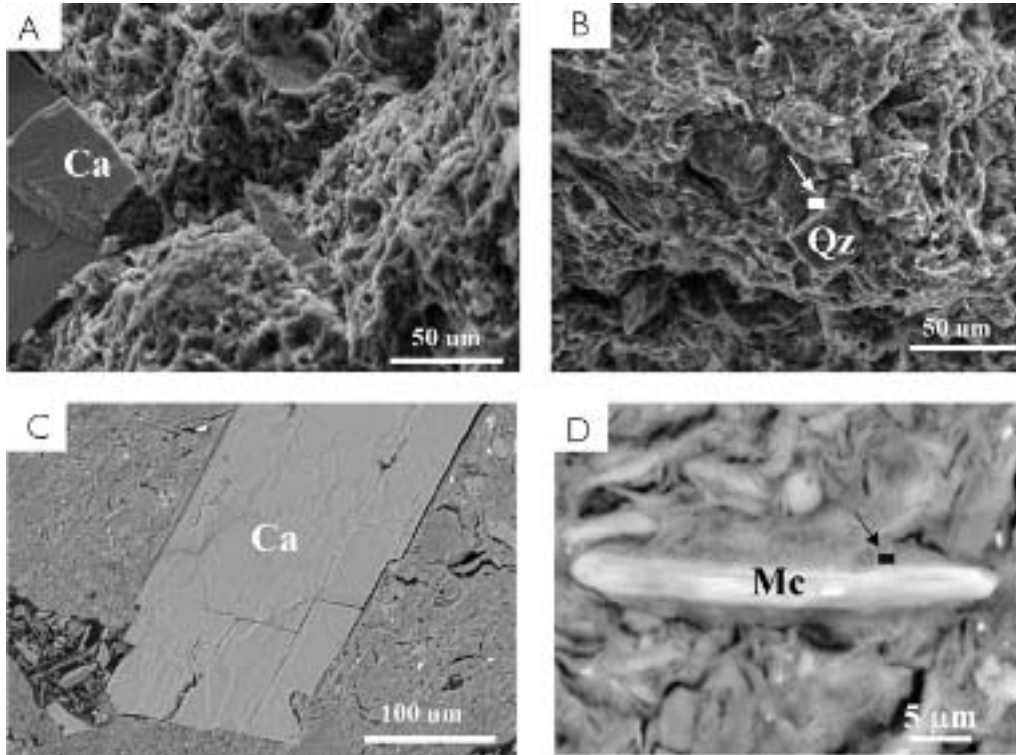


Figure 1 (A) A secondary electron image of a fragment of sample Part-9, in which calcite grains (Ca) with boundaries defined by rhombohedral cleavage can be seen. (B) A secondary electron image of a fragment of sample PG-1, showing a rough matrix and quartz temper grains (Qz). (C,D) BSE images of sample Part-9: (C) a calcite grain and (D) a mica crystal (Mc) with a brighter, Fe-rich core, immersed in clay matrix. Squares indicate the approximate areas corresponding to low-magnification TEM images.

of the fine-grained matrix show similar and constant compositions, with major amounts of Si, Al and O, and minor amounts of Mg, K, Ca, Fe, P, Cl and Ti. Even though the resolving power of BSE is only  $\sim 1 \mu\text{m}$ , images of polished samples allow individual platy crystals in the fine-grained matrix to be distinguished, such grains having irregular shapes (Fig. 1 (D)). The qualitative compositions, grain sizes and shapes imply that the matrices consist largely of clay minerals (phyllosilicates), which have undergone no or little alteration. Dolomite and zircon crystals  $<1 \mu\text{m}$  in size were also identified as minor phases. Elongated pores,  $5 \mu\text{m}$  long, and thin cracks around coarse grains were also observed in BSE images.

The other samples, which were subjected to higher temperatures, show a range of microtextures that are entirely different from those previously described. As in the low-temperature samples, coarse grains, mainly quartz and mica, were imaged. In contrast to lower-temperature samples, however, relict muscovite crystals do not show sharp contacts with the matrix, and the matrix appears to be homogeneous, with no individual clay mineral grains being discernible in either SE or BSE images, even though SE images can resolve features as small as a few tens of angstroms in size. EDS analyses of large mica grains are consistent with a muscovite-like composition, as in low-temperature samples. SE images show the presence of spheres, *c.*  $60 \mu\text{m}$

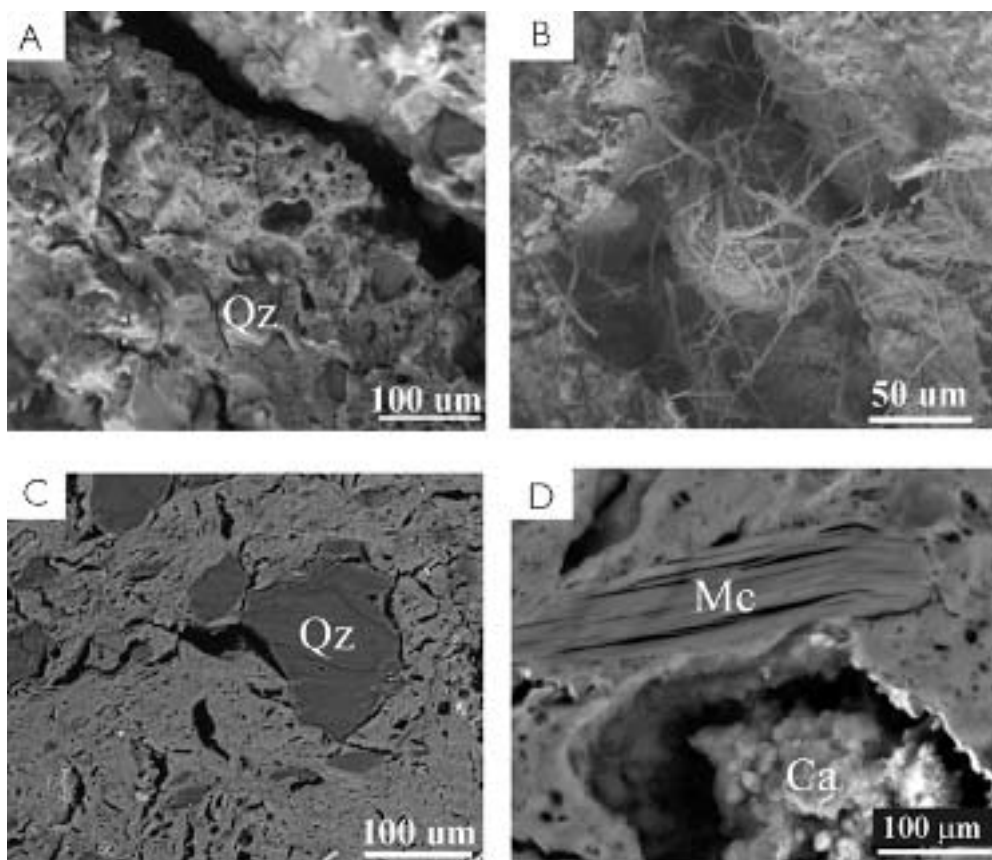


Figure 2 Secondary electron images of sample Part-25. (A) Pore-space and quartz temper within the clay-rich matrix. (B) Spheres and filaments in a large void within the clay-rich matrix. (C, D) BSE images of sample Part-25: (C) quartz grains in a uniform matrix; (D) a muscovite crystal, showing sharp contact with matrix and calcite filling pores.

in diameter, filaments up to 200  $\mu\text{m}$  long, and abundant rounded pores ranging from  $<1 \mu\text{m}$  to 50  $\mu\text{m}$  in diameter (Figs 2 (A) and (B)). Some of the pores are lined with calcite and Fe oxides (Fig. 2 (D)). The higher-temperature samples have a smooth, uniform texture as seen in SE images, in contrast to the rough texture shown by lower-temperature samples. BSE images of a polished thin section (Fig. 2 (D)) display the detailed texture of a sherd in sample Part-25. Elongated micron-sized pores, randomly distributed, large quartz grains and relict mica grains can be observed within the matrix. Other significant features in the high-temperature samples include tiny (5  $\mu\text{m}$ ) crystals in sample PG-4, which were tentatively identified as gehlenite on the basis of EDS analysis, and features typical of corrosion on the surfaces of calcite grains in sample CP-11.

#### *Transmission electron microscopy (TEM)*

Because TEM is such a high-resolution technique, observation of even millimetre-sized samples is time-consuming. We therefore selected samples from the low- to high-temperature ( $<900^\circ\text{C}$ )

sets that had been found to be representative on the basis of XRD, optical and SEM data. TEM images are shown in Figures 3–8. Figures 3 (A) and (B) show TEM images of the low-temperature sample, Part-9, Figure 3 (A) being a low-resolution TEM image of the clay-rich matrix. The plane of the image is perpendicular to the layering of the clay minerals. The sub-parallel clay layers comprise continuous ‘packets’ of layers which are up to 300 nm thick. The packets have curved layers and are separated by elongated voids. These are identical to voids formed on shrinkage of clay minerals that have become dehydrated due to heating. Extensive areas of clay minerals give selected area electron diffraction (SAED) patterns that show that they have a crystalline structure despite having undergone at least partial dehydration. The SAED patterns show reflections that are typical of 1M<sub>d</sub> and 2M polytypes of clays, having layers with ~10 Å spacing. That spacing implies members of the smectite(dehydrated)–illite–muscovite clay-mineral series when combined with the EDS analyses, which shows them to be relatively rich in Al, rather than in Fe and/or Mg (Table 2). The area of interaction of the sample and

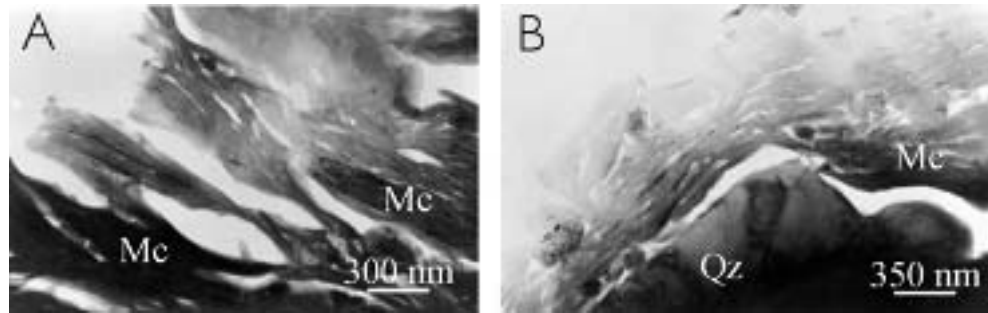


Figure 3 (A) A low-resolution TEM image of the matrix of sample Part-9, showing clay minerals with layers oriented normal to the image, and separated by lenticular voids caused by dehydroxylation. (B) A low-resolution TEM image of a portion of a silt-sized quartz grain surrounded by a matrix of dehydroxylated clay minerals.

Table 2 The chemical composition of micas from sample Part-9 and amorphous areas and micas of sample Part-25

	Part-9							Part-25			
	1	2	3	Ms 4	5	6	7	Am		Ms	
	1	2	3	4	5	6	7	1	2	1	2
Si	6.57	6.88	6.78	6.55	6.26	5.68	5.81	5.83	5.93	6.21	6.70
Al(IV)	1.43	1.12	1.22	1.45	1.74	2.32	2.19	2.17	2.07	1.79	1.30
Al(VI)	2.53	2.45	3.03	2.17	3.20	3.45	3.50	2.25	2.56	1.90	3.30
Mg	1.01	0.83	0.72	0.82	0.58	0.38	0.35	0.41	0.37	0.50	0.00
Fe	0.40	0.57	0.25	0.92	0.18	0.16	0.16	0.98	0.86	0.88	0.30
Ti	0.00	0.00	0.00	0.00	0.00	0.00	0.00	0.00	0.00	0.00	0.00
Ca	0.07	0.15	0.00	0.09	0.05	0.00	0.00	0.29	0.21	0.71	0.40
Na	0.80	0.65	0.51	0.39	0.37	0.35	0.44	0.33	0.00	0.00	0.48
K	0.87	0.76	0.80	1.01	0.88	0.95	0.85	0.44	0.67	0.80	0.36

All analyses have been normalized to six cations. All Fe is assumed to be ferrous iron. Am, amorphous area; Ms, muscovite; Al(IV), tetrahedral Al; Al(VI), octahedral Al.

electron beam, for the purposes of obtaining EDS data, may be made as small as 10–20 nm, approximately 100 times smaller than that even of an SEM. The small domains shown in Figure 3 (A) are thus large compared with the areas included within the chemical analysis. The grains that show ordered two-layer polytypes through well-defined, periodic reflections in SAED patterns are muscovite, whereas those that show considerable disorder in layer stacking are members of the smectite–illite clay-mineral series. Muscovite and smectite–illite also differ in that muscovite has a larger grain size and a higher proportion of Al relative to Si.

The large (temper) grains immersed in the clay matrix cannot be imaged because they are too large relative to the areas that can be included within the area of the electron beam of the TEM. Nevertheless, Figure 3 (B) shows a portion of a silt-sized quartz grain surrounded by the matrix, which is comprised of clay minerals. The clay minerals have been separated from the quartz grain due to shrinkage of the clays. Some large grains (Fig. 4 (A)) show cracks and contrast due to defects, assumed to be strain as a result of expansion on heating. Figure 4 (B) shows areas of the clay matrix with a uniform grey contrast, within which there are both voids (white) and 4–5 nm thick linear units with a dark contrast (black arrows). The uniform, grey areas give no diffraction pattern and therefore are not crystalline. By contrast, the dark linear units within the grey areas, and occurring as separate dark packets, give SAED patterns that correspond to the 10 Å spacing of the smectite–illite–mica series (Fig. 4 (B), inset). However, AEM analyses of the grey areas correspond to mica. Table 2 shows the chemical composition of the clay-rich matrix from sample Part-9. Those data collectively indicate that the materials shown in Figure 4 were entirely composed of clay minerals before firing, but that dehydration during firing caused some, but not all, of the clay minerals to become amorphous (Fig. 4 (B)).

The low-temperature samples are also characterized by the presence of rounded domains less than 10 nm in size, which are intergrown with thick packets of mica (Fig. 5). AEM analyses show the presence only of iron and oxygen, but no reflections were observed in SAED patterns. Such material is commonly observed as a product of weathering, and corresponds to the mineral goethite, FeO(OH), for which Fe is in the oxidized state.

As shown in the upper part of Figure 6 (A), the clay-rich matrix of the higher-temperature samples (Cp-11 and Part-25) has a homogeneous appearance, within which individual grain outlines and even the direction of layering of the original clay minerals cannot be observed. Such areas contain rounded ‘bloated’ pores ranging up to several nanometres in diameter. SAED patterns give no diffraction spots, which implies that the material is amorphous. AEM analyses (Table 2) show that the composition is like that of the clay observed in lower-temperature samples. Such areas are typical of all of the matrix of the two high-temperature samples.

On the other hand, the large grains of quartz and mica can still be recognized. For example, a large, damaged mica grain  $\sim 1 \mu\text{m}$  in thickness is indicated by white arrows in the lower half of Figure 6 (A). SAED patterns display the typical 001 series of diffraction spots, having a periodicity of 1 nm, straight 001 lattice fringes, with 1 nm lattice fringes in high-resolution images, and AEM data consistent with muscovite mica. On the other hand, the image shows elongated pores that are inferred to result from shrinkage that occurred during dehydroxylation, and lattice fringes can be seen only in portions of the crystal. Those relations imply that parts of the crystal have been severely damaged during heating, but that some parts have escaped significant change. Images of large quartz grains (not shown) show that grains have thin rims with a contrast different than that of the interiors of grains. These are inferred to correspond to the inversion of quartz to cristobalite or tridymite due to higher temperatures encountered in grain rims during heating.

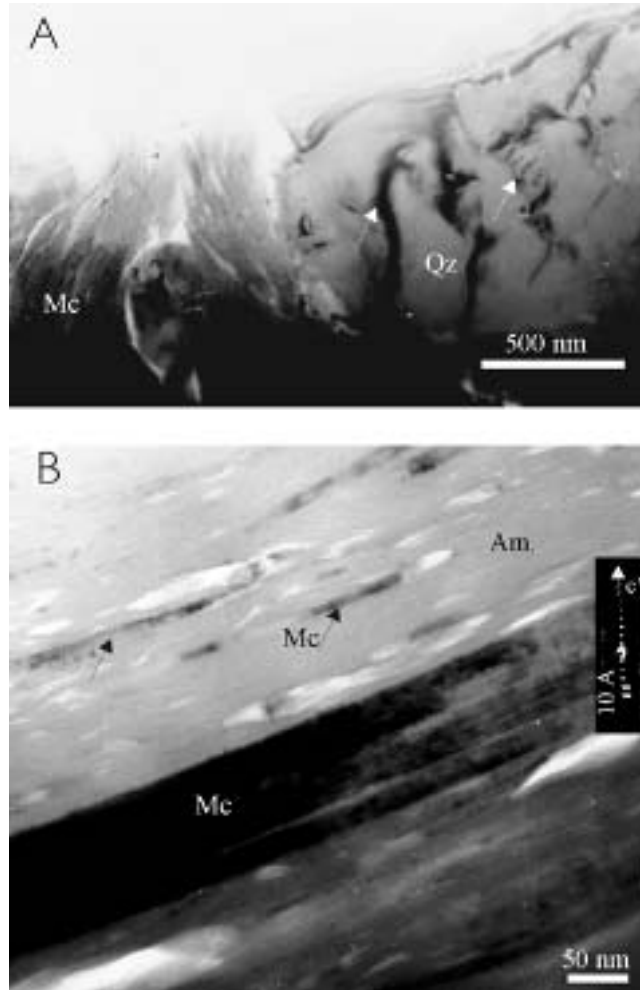


Figure 4 TEM images of sample Part-9. (A) A low-magnification TEM image: the right-hand part of the image shows a silt-sized quartz grain, in which strain-contrast features in quartz due to stress during the firing process can be seen (white arrows). The left-hand part of the image shows the clay-rich matrix. (B) A lattice-fringe TEM image with a large muscovite packet, relict muscovite within dehydroxylated mica (black arrows) and porous amorphous matter (Am). Inset: a selected-area diffraction pattern with the characteristics of 1 nm periodicity of muscovite.

Areas of sample Part-25 show small crystals immersed in a homogeneous matrix which gives no diffraction pattern (Fig. 7) and which is inferred to be highly altered clay. The crystals give SAED patterns consistent with single crystals. Analysis of the diffraction relations ( $d$ -values and inter-vector angles) gives values consistent with the pyroxene family of minerals. Chemical analyses free of contamination of the matrix could not be obtained, however, so the exact species of pyroxene could not be determined. These crystals had not been previously detected by XRD, because their relative proportion was much less than the detection limits of XRD.

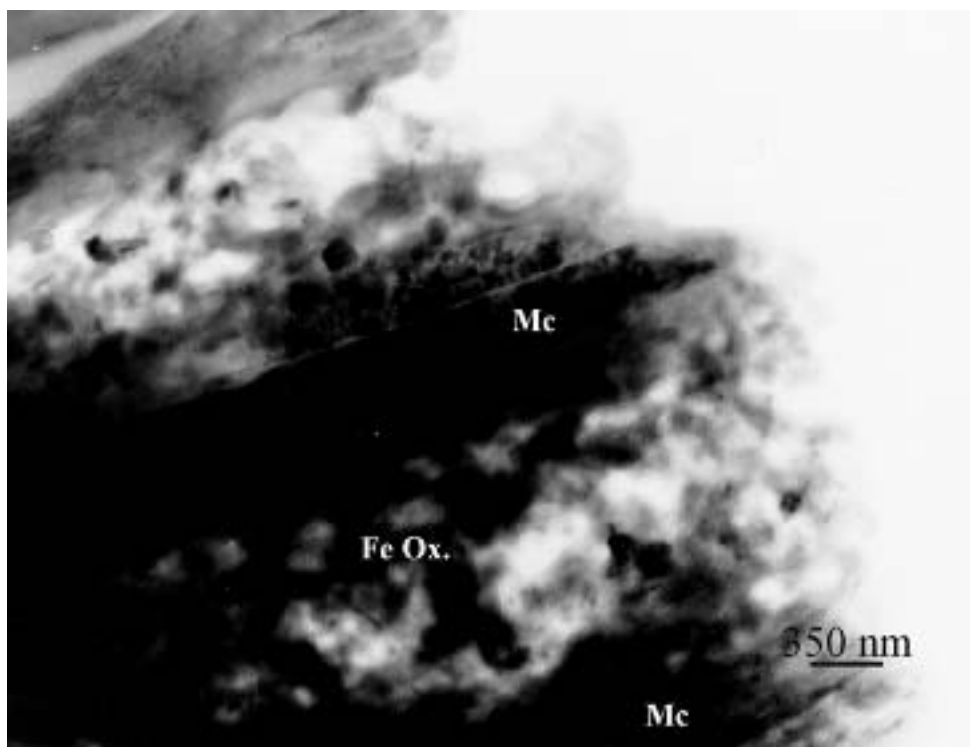


Figure 5 A low-magnification TEM image of sample Part-9: irregular rounded patches of goethite (Fe Ox.) within the void space between packets of muscovite (Mc).

Figure 8 shows a TEM image of a large mica-like crystal, which gives SAED patterns consistent with  $2M_1$  polytypism, and which has sharp 00l lattice fringes with 1 nm spacings. Such data are consistent with undamaged muscovite mica. It is surrounded by material with contrast variations parallel to the length of the cross-section of the muscovite crystal. Some of this material gives no diffraction and therefore gives no lattice-fringe images; that is, it is amorphous due to heating. But some areas have lattice fringes that have *c.* 1 nm periodicity, are curved and anastomosing, and are surrounded by amorphous matter. The latter features are typical of smectitic clay whose inter-layer water has been lost due to heating, resulting in collapse of layers from 1.2–1.3 nm to 1 nm. These relations are consistent with an intermediate degree of damage, in which the matrix is largely but not entirely altered, but with large crystals that have suffered little damage.

#### DISCUSSION

##### *A comparison of the evolution of textures and mineralogy as observed by SEM and TEM*

The optical and SEM study showed that the samples consist of very fine-grained, clay-rich matrix in which are immersed large grains (temper) of very different minerals, predominantly quartz, mica and calcite. The large grains are dominantly quartz, but those in sample Part-9 are

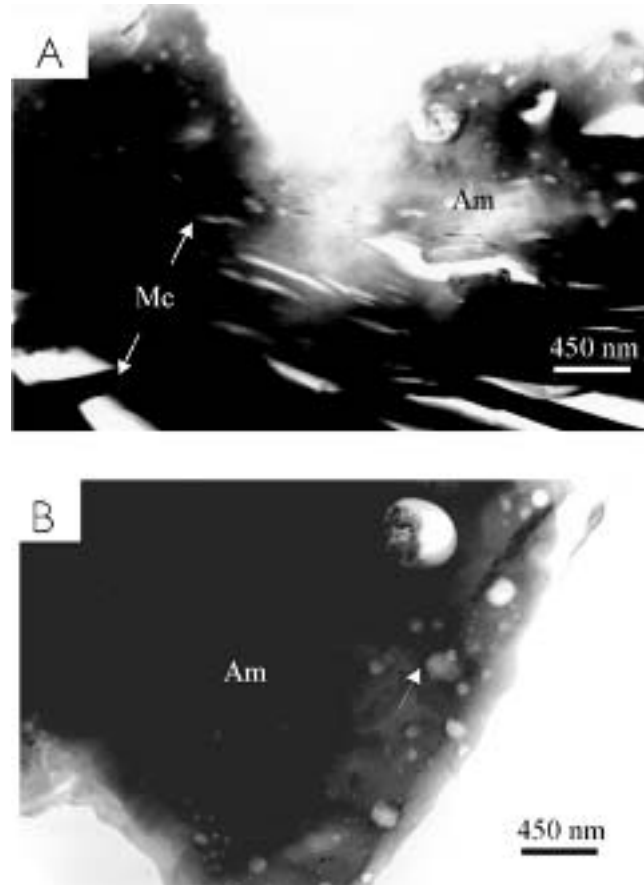


Figure 6 Low-magnification TEM images of sample Part-25. (A) The upper part of the image shows an amorphous area with rounded pores. The lower part shows a thick relict mica crystal (white arrows) with shrinkage cracks due to dehydroxylation. (B) An area showing rounded 'bloated' pores within homogenized, amorphous matrix.

calcite. Although the low-resolution SEM and optical images indicated that large mica grains were unaffected by firing, TEM images showed elongated features with dark contrast parallel to mica layers (Fig. 4). Such features are consistent with strain in the structure as caused by expansion during the onset of heating, preceding major changes as occur with dehydroxylation. A TEM study of large muscovite grains in sample Part-9 also showed the presence of shrinkage cracks consistent with at least partial dehydroxylation, but SAED patterns had sharp 001 reflections, with 1 nm spacing typical of untransformed material. Those relations demonstrate a stage in heating that is somewhat more advanced than that shown by the simple stress noted above; that is, limited parts of a given grain were affected by dehydroxylation, but with most of the grain remaining untransformed. Given a possible range from no effect to complete dehydroxylation such information regarding the degree or duration of heating is typical only of high-resolution TEM data.

SEM images show that the large temper grains are surrounded by a material that resembles fine-grained clay minerals. Corresponding EDS analyses are quite variable from point to point,

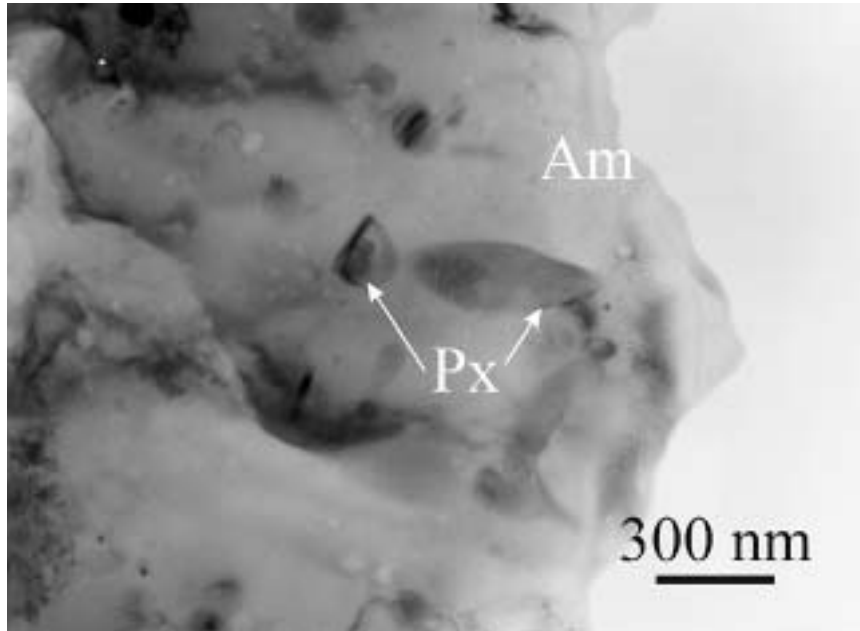


Figure 7 A low-magnification TEM image of pyroxene crystals (Px) (white arrows) in a homogeneous matrix of amorphitized clay (Am).

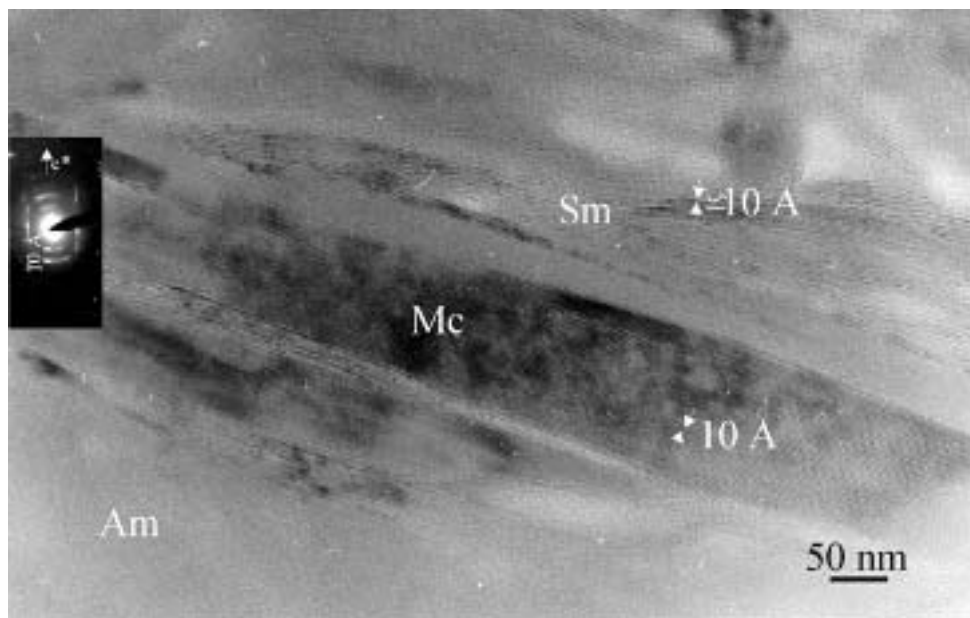


Figure 8 A lattice fringe TEM image of a muscovite crystal with characteristic 1 nm periodicity surrounded by amorphous material, and curved layers with c. 1 nm periodicity, typical of collapsed smectitic clay (Sm).

which is consistent with heterogeneous material. EDS analysis in the SEM can only resolve grains greater than  $\sim 1 \mu\text{m}$  in size. Nevertheless, the qualitative EDS analyses reflect an average composition dominated by the O, Si, Al and K, which is consistent with significant amounts of clay minerals such as smectite, interstratified illite/smectite (I/S), illite or muscovite, but also with lesser amounts of other minerals, including perhaps quartz. In sharp contrast, TEM study of the matrix of sample Part-9 easily resolved the different phases in the matrix. EDS analyses on small areas allowed us to directly identify the dominant clay mineral as particular varieties of smectite, either montmorillonite or beidellite and minor illite. The electron diffraction data show that both  $1M_d$  and  $2M$  polytypes (layer stacking sequences) are present in different particles. The former is consistent with smectite and the latter with muscovite mica. The collective data therefore indicate that the clay minerals in the matrix are a complex mixture of muscovite, illite and smectite, but that the latter is the dominant phase.

The presence of the well-defined diffraction patterns of  $1M_d$  and  $2M$  diffraction patterns implies that grains that gave such patterns have not been subject to intense heating, especially with respect to dehydroxylation. On the other hand, images of other grains display abundant lenticular shrinkage cracks. The presence of diffraction patterns implies that the basic structure of at least most of the clay minerals of the matrix has been preserved, even though the large volume of pore space (see, e.g., Fig. 3 (A)) is consistent with massive shrinkage. Smectite loses water in two steps. In the first, which occurs at less than  $100^\circ\text{C}$ , inter-layer water is lost. But such loss is reversible, and therefore inter-layer water would be regained when pottery fragments were subjected to moisture during burial, with shrinkage cracks probably being healed. On the other hand, irreversible shrinkage implies loss of water through dehydroxylation, which first occurs without complete destruction of the crystal structure. The diffraction data imply that the basic mica structure was retained. These relations therefore imply a temperature in the approximate interval of  $700\text{--}1000^\circ\text{C}$  (see below for discussion of change in structure as a function of temperature).

SEM-BSE images of selected high-temperature samples, Part-25 and CP-11 (Fig. 2), illustrate the effects of increasing firing temperature, estimated to be less than  $850^\circ\text{C}$ . The large temper grains appear to be little changed relative to the lower-temperature material, grains having retained their angular shape. Nevertheless, in the TEM study, some quartz grains show rims with different contrast. These could not be analysed in detail, but such features can be produced either by chemical reaction with the matrix or by inversion of quartz to the polymorph tridymite or cristobalite. The latter is probable, as it is compatible with the observations of Clark and Peacor (1992) for quartz grains heated and inverted during pyrometamorphism.

In SEM images (Fig. 2), large muscovite grains display dark bands parallel to layering and the matrix shows variations in contrast that have a 'wormy' appearance. Study by TEM showed, however, that the basic crystal structure of some parts of large mica grains was destroyed, but the presence of some 001 lattice fringes shows that limited volumes in the interior of grains retained their basic structure. The solid material, on the other hand, is homogeneous in appearance, by contrast with lower-temperature material (Fig. 2 (C)). The collective SEM data are consistent with nascent vitrification, as suggested by Maniatis and Tite (1981), with a firing temperature below  $850^\circ\text{C}$ . The matrix of the higher-temperature samples, as imaged by TEM, shows little of the characteristics of clay minerals, except for elongated shrinkage cracks which appear to be parallel to a pre-existing layer structure, and the presence of diffraction data limited to small, localized volumes. The latter indicate that the basic 2 : 1 units of clay minerals have been retained, but only locally. The bulk of the matrix, including that which is adjacent to shrinkage cracks, appears to be homogeneous in texture, except for the presence of sub-spherical 'bloated pores'.

The latter are interpreted to be the remnants of vapour-filled pores, the vapour resulting from dehydration. The EDS analyses are similar to those for clay-rich areas in the low-temperature areas. Most material gives no electron diffraction, indicating an amorphous material. These data collectively indicate that the clay and other minerals of the fine-grained matrix have undergone destruction of structure and diffusion of elements, to form a homogeneous, amorphous material that grew around included vapour derived from the hydroxyl component of the original clay mineral. TEM study also showed the local formation of euhedral pyroxene crystals, not detected previously by XRD or SEM, and representing the most advanced state of alteration of the parent matrix material.

*TEM textures in clay minerals as a consequence of firing: implications for estimation of the duration of firing*

The degree of reaction that occurs in and amongst the original materials used to manufacture pottery depends primarily on two variables, temperature and time. Determination of temperature may generally appear to be well-defined by the presence of a phase known to be stable only above a certain temperature, but the reaction by which that phase forms requires time. Chemical reactions between phases require diffusion of reactant ions, and the rate of diffusion therefore limits the rate at which new phases form. Firing of pottery, on the other hand, occurs over short time intervals, for which reactions may not go to completion; indeed, if the duration of the maximum firing temperature is short enough, temperatures may be greater than those necessary to promote formation of reactants due to sluggishness of reaction.

The features of TEM images of the matrix of low-temperature samples showed shrinkage cracks implying dehydration and minor dehydroxylation, but the presence of the diffraction patterns showed either that some portions of such grains were not affected by loss of hydroxyl, or that the basic 2 : 1 units of mica structure were so little damaged that there is still periodicity in the structure. The large muscovite grains have developed lenticular pores due to contraction caused by dehydroxylation, but they also retain an ordered structure. Likewise, the large temper quartz grains show the effects of strain due to thermal expansion.

The high-temperature samples have a matrix that is largely homogeneous and amorphous. Such amorphous material need not be 'glass' in the usual sense, as it is not derived by rapid cooling of a melt. Rather, it may be derived by destruction of the clay-mineral structure and solid-state or vapour-aided diffusion of chemical components, as facilitated by the disordered structure. Although the matrix may show linear features corresponding to the former layering of the clay minerals as seen in projection, no SAED patterns can be seen, and the composition as determined by high-resolution AEM analyses is relatively uniform. Such material corresponds to the complete breakdown of the mica structure, and homogenization of composition through diffusion. Nevertheless, some small volumes give 001 SAED patterns, and the corresponding TEM images display 001 lattice fringes that reflect local order of the 2 : 1 clay-mineral structure.

The presence of 'bloated pores' implies local growth of the amorphous matrix material around vapour bubbles, as compared with the lenticular voids produced by delamination of clay-mineral layers at lower temperatures, or locally in the higher-temperature samples, which reflect stress caused by shrinkage. The large temper grains, on the other hand, retain their morphology, including the elongated shape of pores produced by delamination. The crystalline structure has been partially destroyed, as demonstrated by the lack of SAED patterns, but homogenization has not occurred as in the matrix clays minerals. Some of the temper quartz grains also display contrast in TEM images on the rims, implying local inversion to tridymite or

cristobalite. The lack of complete inversion of grains implies that only grain rims were subjected to temperatures high enough to promote inversion.

These relations collectively imply that the matrix achieved higher temperatures than the large temper grains, and that in both matrix and temper grains, the temperature was not uniform. The difference in thermal effects in matrix and temper is compatible with the larger volume of pore space created by dehydration of inter-layer water of the smectite component of the matrix, as opposed to the smaller volume change associated with dehydroxylation of both matrix and temper at high temperatures. Dehydration of smectite produces both the water vapour itself and the space for its transport. Transport of heat via vapour would enhance homogenization of temperature. Worden *et al.* (1987) studied pyrometamorphic rocks and they concluded that the vapour phase that was produced in the breakdown of phyllosilicates can promote the melting of quartz and albite grain boundaries, the presence of a melt thus enhancing diffusion and reactions between grains. In the materials characterized in this study, temperatures were insufficient to cause melting, but the conclusions regarding transport via a vapour phase as noted by Worden *et al.* (1987) are nevertheless applicable.

The relations described above reflect an abbreviated duration of firing in the samples of this study. If calibrated with known heating temperatures and durations in experiments, or when compared with materials from other sites that have different durations of firing, such relations have the potential to provide an insight into the specific conditions of firing at given sites, as well as for direct comparison of characteristics of materials from different sites.

The process by which muscovite mica—and, by inference, the related clay minerals smectite and illite—change as a function of temperature has been intensively studied both by experiment and by observation of natural materials. Recent experiments have shown that muscovite dehydroxylates between *c.* 700°C and 1000°C (Mazzucato *et al.* 1999, and references therein). They also show that original muscovite can coexist with dehydroxylated muscovite, which gives rise to diffraction patterns, and amorphous material. Clark and Peacor (1992) studied pyrometamorphic rocks and covered a more extensive temperature range, up to 1300°C. They observed that, following delamination and amorphitization of the illite-rich matrix, mullite crystals were observed to grow within the amorphous equivalent of clay. Such a process requires diffusion of Al and Si in the solid state, a process that is very sluggish. The mixture of mullite, amorphous material and other crystalline phases was observed to have melted in the sample subjected to the highest temperatures, with the formation of crystalline compounds and, subsequently, glass upon cooling. All of the latter materials were observable only by TEM.

The sequence of materials observed by Mazzucato *et al.* (1999) and Clark and Peacor (1992) is directly analogous to that observed in pottery in the present study, with the exception that the starting clay material for manufacture of pottery apparently included smectite, which to a first approximation, has a 2 : 1 structure like that of muscovite, but with sheets of water molecules. Such water is lost at very low temperatures, <100°C, with retention of the basic structure. Dehydroxylation commenced in matrix clay minerals at *c.* 700°C, with retention of the basic 2 : 1 structure, but continued to higher temperatures with coexisting hydroxylated and dehydroxylated layers. Matrix clays were largely homogenized and amorphitized at the highest temperatures, < 1000°C. The temperatures corresponding to the formation of mullite were apparently not achieved, nor were those corresponding to melting and to the subsequent formation of glass. However, the temperature was locally sufficient for the growth of pyroxene within the amorphous matrix. Such amorphous material is not glass *sensu strictu*, since glass, which is derived by cooling of a melt, has a local crystal structure reflecting that of the melt from which it is derived. The amorphous material in the fired pottery is derived via vapour-mediated, solid state reactions, and is inferred to have a local structure that mirrors that of its predecessor clay.

*The use of TEM to determine the firing temperature*

The most widely applied methods for determining the firing temperature of ancient pottery concern the application of 'mineralogical thermometers', with mineral assemblages as determined primarily by XRD. Schomburg (1991) recommended the use of thermal reactions (dehydroxylation, decomposition, formation of high-temperature phases and morphological changes) as 'archaeological thermometers'. In the absence of characterization of textures at high magnifications, one of the difficulties in the use of such features is related to the question of disequilibrium (Riccardi *et al.* 1999). That is, methods such as XRD integrate data over an entire sample, including all stages of reaction progress. Glass and amorphous matter are not detectable by XRD, and even methods such as optics and SEM, which define gross textures, generally cannot differentiate between amorphous materials formed below temperatures of melting and glass produced by quenching of a melt, for example. As illustrated by the TEM observations of this study, there are abundant relations that can only be detected by imaging textures at high resolution and determining the textural relations among those minerals, which are abundant enough to be detectable with methods such as XRD. The dynamics of firing, including temperature, duration of firing and rate of cooling, directly affect features such as the nucleation and growth of new phases, reaction process and many other relations, as illustrated in the TEM observations described above. TEM is also a useful tool to determine polymorphic changes suffered by the temper grains due to the firing process.

The difference in estimated firing temperatures determined by XRD and TEM for sample Part-9 further illustrates the power of TEM in determining relations for specific small volumes as opposed to the averaging effect over heterogeneous materials by XRD. That is, partial dehydroxylation of matrix clays was determined by TEM, implying a maximum temperature of *c.* 700°C, whereas XRD data implied a temperature of *c.* 450°C. As shown by TEM, the matrix clay was indeed largely unaffected by higher temperatures, so that the average material sampled by XRD contained a very small component of the material altered at highest temperatures.

*TEM observations of post-depositional alteration features*

In the studied samples, some oxides have been detected and the relations described herein imply an origin due to weathering while buried in soil. Figure 5 shows goethite, a mineral that is known to commonly form due to alteration of iron-containing minerals, incompletely filling the void spaces between packets of muscovite. That texture is strikingly similar to those illustrated by Giorgetti *et al.* (2000) for near-surface alteration and, by analogy, this strongly implies that the goethite was produced during the burial of sherds.

Changes that occur subsequent to firing and during burial of pottery sherds may result in erroneous conclusions resulting from 'mineralogical or archaeological thermometers' in the absence of high-resolution textural relations. For example, the alteration of thermodynamically unstable and reactive amorphous matter in contact with water or hydrothermal solutions is one of the main causes of smectite genesis in natural environments (Tazaki and Fyfe 1989; Banfield *et al.* 1991). Such reactions may occur during burial of sherds that contain amorphitized clay minerals through interaction with pore fluids. Indeed, on the basis of XRD data, neoformed smectitic material in ancient pottery has been reported as occurring in ancient pottery (Capel *et al.* 1985; Nagasawa and Ohkochi 1988), as a result of interaction of the fired material with meteoric water or groundwater. TEM images of such material show very characteristic textures, where the secondary smectite is seen to grade directly into, and be derived from, amorphous material (see, e.g., Alt and Mata 2000; Bauluz *et al.* 2000). Such textures are strikingly different

from those shown in Figure 8, for example, which have characteristically wavy layers of collapsed smectite (~1 nm), in packets less than 10 nm thick within an amorphous phase around mica-like crystals, verifying an origin during firing. Such textural information is vital for determining the origin of smectite, for example, because X-ray diffraction data of bulk samples cannot generally differentiate between origins.

In addition to re-hydration, re-hydroxylation and calcite formation are also possible after firing, and expandable clay minerals can apparently be detected after heating to temperatures up to 800°C, because of re-hydroxylation processes (Emmerich *et al.*, 1999; Muller *et al.* 2000, and references therein). For ancient pottery, Shoval *et al.* (1991) suggested that the amount of re-hydroxylation in ancient materials may be related to the size of the former clay minerals and the degree of crystallinity in the raw materials. Textural relations, especially of clay minerals, are only observable by TEM imaging. It is essential to obtain such data to discriminate between clay minerals, for example, which may be altered by the firing process *vis-à-vis* neoformation and rehydroxylation during burial. Although carbonates such as calcite may irreversibly be decarbonated, the resulting calcium oxide may react with CO<sub>2</sub> in groundwater to form new calcite. Such calcite could generally not be differentiated by XRD from original calcite in fired material, but it would have very characteristic features, as observed with TEM.

#### *TEM and provenance studies*

Determination of the origin of raw material used in the manufacture of artefacts is an important goal in the study of pottery. These studies are mainly based on the nature and composition of temper grains as seen by optical microscopy, scanning electron microscope analysis and electron microprobe analysis (Freestone 1982).

In the present study, samples came from settlements located in the northwestern part of the Iberian Chain, the Cameros Basin, where abundant thick strata of limestones, sandstones and pelites (shales and slates) of Mesozoic age occur (Mata Campo 1997). Optical and SEM observations show that calcite temper grains have angular shapes with the regular morphology of rhombohedral cleavage fragments, clearly demonstrating that they result from grinding of larger samples. In addition, they are pure minerals rather than mineral assemblages, implying that the source materials were larger monomineralic samples that had been ground into smaller fragments. It is the rule, rather than the exception, that grains of minerals that appear to be pure at the optical or SEM scale are observed by TEM to have inclusions of other minerals. Such inclusions may be diagnostic of provenance when observed. On the other hand, the unusual purity of calcite observed in this study requires a source where coarse, pure calcite was available, not calcite—for example, from limestones. Quartz temper grains are rounded, however, which is inconsistent with the breakage of larger grains, and implies wear by natural processes. Such quartz is common in sands and gravels and, unfortunately, is therefore widespread. The temper of the samples described in this study is striking in the limited number of minerals. Sands and gravels and other environments where rounded quartz occurs generally are heterogeneous with a variety of minerals such as feldspar, and with a single mineral varying in composition. Although the presence of only homogeneous quartz, muscovite and cleaved calcite does not point to a single locality, these minerals do severely restrict the general nature of the source(s).

The fine-grained matrix was heterogeneous with dominant smectite and minor illite as well as lesser amounts of quartz and muscovite. That assemblage is typical of some shales, a rock type that is common in the Ebro Basin. However, shales may be comprised of a great variety of minerals in addition to the minerals observed in this study, and the lack of minerals such as

feldspar, calcite or chlorite, despite observations at the TEM scale, severely restricts the origin of the matrix. Nevertheless, the observed assemblage is not uncommon, so the specific site cannot be identified.

#### *Archaeometric considerations for the case study*

The analysed sherds from the megalithic ensemble of Peña Guerra (Nalda, La Rioja) are Bell Beaker ceramics corresponding to the grave goods of the intrusive Beaker inhumations in three megalithic buildings: Peña Guerra I (samples PG-1 and PG-2), Peña Guerra II (sample PG-4) and Peña Guerra III (sample PG-6). Only Peña Guerra II had not been disturbed before the archaeological excavations (Pérez Arrondo 1987). The results clearly show the distinctive features of those obtained from sample CP-11 (Collado Palomero, Viguera, La Rioja). This sherd was found below the level of the megalithic burial. Typologically, it belongs to the Late Neolithic. The imaged digital analysis showed a distinctive feature of the distribution of the temper grains (Gallart-Martí and Mata 1995), but only with TEM analysis has a mineralogical and microstructural characterization been possible.

Partelapeña (El Redal, La Rioja) is a prehistoric settlement where stratigraphic levels have been recognized (Álvarez Clavijo and Pérez Arrondo 1988). The evolution in the technology of the pottery can be observed in the results of the three samples. Sample Part-9, from lower level I, is a coarser sherd fired at lower temperature. Sample Part-15 comes from level III, where excised pottery is common. A fire probably destroyed the settlement at this level. Later, in upper level IV, excised ceramic was not deposited. It is difficult to know if a new group of people occupied this archaeological level. The obtained TEM results show that the higher temperature reached in the firing of the pottery can be related to a new technology of making pottery.

#### CONCLUSIONS

The use of TEM techniques provided detailed characterization of microtextures of selected ceramic materials, resulting in definition of the processes that occurred during the transition from starting materials to extensively amorphitized clay minerals and newly crystallized phases.

In low-temperature materials, intermediate phases produced in the firing process, most of which had sizes well below that of resolution even by SEM, were identified by TEM. These features give valuable information about factors that affect the temperature and duration of firing of ancient ceramics, in part through definition of the gradient in changes in the same samples, from original materials through amorphitized clay minerals. TEM also provided complementary data on original raw materials and therefore on the characteristics of the source areas.

#### FUTURE RESEARCH

If calibrated with known firing temperatures and durations of experiments, or when compared with materials from other sites, TEM studies can provide valuable data about the mechanism of firing, the estimation of temperature and the duration of firing. This is especially important in prehistoric pottery, where the firing temperature can be low. Chemical compositions of amorphous phases and individual crystals at nanometric scale can also be obtained.

Weathering products originating in soils, as well as the origin of common secondary products in ceramics, as calcite, can be evaluated by analysis of microtextures by TEM. As discussed in

the previous sections, the study of nanometric particles can help to explain superficial properties—such as colour, and so on—found in many objects.

The use of TEM is severely limited by the availability of equipment, and requires special expertise on the part of operators. It is time-consuming and provides results on very small volumes of materials. Therefore, it cannot be used regularly and universally. Nevertheless, as is the case with geological samples, large numbers of samples can first be more readily studied by low-resolution techniques such as XRD and optics, which define the types and ranges of sample characteristics. For specific problems, a small number of representative samples can then be selected and studied in those laboratories where TEM is a standard tool, and where techniques for the characterization of mineralogical materials are well developed.

#### ACKNOWLEDGEMENTS

This study has been supported by National Science Foundation grants EAR 9418108 and 9814391 to D. R. Peacor. We also thank C. Henderson, Li-Shun Kao and Carlos López de Calle for technical assistance with the electron microscope techniques. We thank P. Álvarez Clavijo for supplying some of the archaeological samples. S. Guggenheim kindly provided insights into the process of rehydroxylation of dehydrated I/S.

#### REFERENCES

- Aguarod Otal, C., Feliu Ortega, M. J., and Martín Calleja, J., 1995, Aspectos técnicos de diversas producciones de cerámicas de cocina romana a través de la microscopía electrónica de barrido, in *Proceedings of the European meeting on ancient ceramics* (eds. M. Vendrell-Sanz, T. Pradell, J. Molera and M. Garcia), 169–72, Generalitat de Catalunya, Departament de Cultura.
- Alt, J., and Mata, M. P., 2000, On the role of microbes in the alteration of submarine basaltic glass: a TEM study, *Earth and Planetary Science Letters*, **181**, 301–13.
- Alvárez Clavijo, P., and Pérez Arrondo, C. L., 1988, Notas sobre la transición de la Edad del Bronce a la Edad del Hierro en La Rioja, *Brocar*, **14**, 103–18.
- Banfield, J. F., and Eggleton, R. A., 1988, A transmission electron microscope study of biotite weathering, *Clays and Clay Minerals*, **36**, 47–60.
- Banfield, J. F., and Eggleton, R. A., 1990, Analytical electron microscopy studies of plagioclase, muscovite and K-feldspar weathering, *Clays and Clay Minerals*, **38**, 77–89.
- Banfield, J. F., Jones, B. F., and Veblen, D. R., 1991, An AEM-TEM study of weathering and diagenesis, Albert Lake, Oregon: I. Weathering reactions in the volcanics, *Geochimica et Cosmochimica Acta*, **55**, 2781–98.
- Barber, D. J., and Freestone, I. C., 1990, An investigation of the origin of the colour of the Lycurgus cup by analytical transmission electron microscopy, *Archaeometry*, **32**, 33–45.
- Bauluz, B., Peacor, D. R., and Elliott, W. C., 2000, Coexisting altered glass and Fe–Ni oxides at the Cretaceous–Tertiary boundary, Stevns Klint (Denmark): direct evidence of meteorite impact, *Earth and Planetary Science Letters*, **182**, 127–36.
- Brearley, A. J., 1987, A natural example of the disequilibrium breakdown of biotite at high temperature: TEM observations and comparison with experimental kinetic data, *Mineralogical Magazine*, **51**, 93–106.
- Capel, J., Huertas, J., and Linares, J., 1985, High *T* reactions and use of Bronze Age pottery from La Mancha, Central Spain, *Mineralogica et Petrographica Acta*, **29**, 563–75.
- Clark, B. H., and Peacor, D. R., 1992, Pyrometamorphism and partial melting of shales during combustion metamorphism: mineralogical, textural, and chemical effects, *Contributions to Mineralogy and Petrology*, **112**, 558–68.
- Edwards, W. I., and Segnit, E. R., 1984, Pottery technology at the chalcolithic site of Teleilat Ghassul (Jordan), *Archaeometry*, **26**, 69–77.
- Emmerich, K., Thule, F., and Khar, G., 1999, Dehydroxylation behavior of heat-treated and steam-treated homoionic *cis*-vacant montmorillonites, *Clays and Clay Minerals*, **47**, 591–604.
- Fabbi, B., 1996, Application of SEM/EDS analysis for studying ceramic materials of archaeological interest, in *Advances in clay minerals, Proceedings of the Spanish–Italian meeting on clay minerals, Granada* (eds. M. Ortega-Huertas, A. López-Galindo and I. Palomo Delgado), 284–7, Sociedad Española de Arcillas.

- Freestone, I. C., 1982, Applications and potential of electron-probe micro-analysis in technological and provenance investigations of ancient ceramics, *Archaeometry*, **24**, 99–116.
- Freestone, I. C., and Middleton, A. P., 1987, Mineralogical applications of the analytical SEM in archaeology, *Mineralogical Magazine*, **51**, 21–31.
- Gallart-Martí, M. D., and Mata, M. P., 1995, Prehistoric pottery from La Rioja (Spain): a textural and mineralogical analysis, in *Proceedings of the European meeting on ancient ceramics* (eds. M. Vendrell-Sanz, T. Pradell, J. Molera and M. Garcia), 61–6, Generalitat de Catalunya, Departament de Cultura.
- Giorgetti, G., Memmi, I., and Peacor, D. R., 2000, Contrast in processes and products of weathering of carpholite and associated phyllosilicates: a TEM study, *European Journal of Mineralogy*, **12**, 33–44.
- Guthrie, G. D., Jr, and Veblen, D. R., 1989, High-resolution transmission electron microscopy of mixed-layer illite/smectite: computer simulations, *Clays and Clay Minerals*, **37**, 1–11.
- Guthrie, G. D., Jr, and Veblen, D. R., 1990, Interpreting one-dimensional high-resolution transmission electron micrographs of sheet silicates by computer simulation, *American Mineralogist*, **75**, 276–88.
- Hochella, M. F., Jr. and Banfield, J. F., 1995, Chemical weathering of silicates in nature: a microscopic perspective with theoretical considerations, in *Chemical weathering rates of silicate minerals* (eds. A. F. White and S. L. Brantley), 354–406, Reviews in Mineralogy, 31, Mineralogical Society of America, Washington, DC.
- Jiang, W. T., Peacor, D. R., Merriman, R. J., and Roberts, B., 1990, Transmission and analytical electron microscopic study of mixed-layer illite/smectite formed as an apparent replacement product of diagenetic illite, *Clays and Clay Minerals*, **38**, 449–68.
- Kingery, W. D., and Vandiver, P. B., 1986, *Ceramic masterpieces*, Free Press/Macmillan, New York.
- Klykova, Y., Mazurkevich, A., and Panteleyev, V., 1998, Image analysis and SEM studies of ancient ceramics and feldspar porcelain structure, *The Americas Microscopy and Microanalysis*, 19–22.
- López de Calle, C., and Ilaraza, J. A., 1997, Fases antiguas del megalitismo de Cameros (La Rioja): caracterización y cronología, in *Coloquio internacional o Neolítico Atlántico e as orixes do megalitismo, Portugal*.
- Lorimer, G. W., and Cliff, G., 1976, Analytical electron microscopy of minerals, in *Electron microscopy in mineralogy* (ed. H.-R. Wenk), 506–19, Springer-Verlag, Berlin.
- Mallory-Greenough, L. M., Greenough, J. D., and Owen, J. V., 1998, Provenance of temper in a New Kingdom Egyptian pottery sherd. Evidence from the petrology and mineralogy of basalt fragments, *Geoarchaeology*, **13**, 391–410.
- Maniatis, Y., and Tite, M. S., 1981, Technological examination of Neolithic – Bronze Age pottery from central and southeast Europe and from the Near East, *Journal of Archaeological Science*, **8**, 59–76.
- Mata Campo, M. P., 1997, *Caracterización y evolución mineralógica de la Cuenca Mesozoica de Cameros (Soria – La Rioja)*, Ph.D. thesis, University of Zaragoza.
- Mazzucato, E., Artioli, G., and Gualtieri, A., 1999, High temperature dehydroxylation of muscovite-2M<sub>1</sub>: a kinetic study by *in situ* XRPD, *Physics and Chemistry of Minerals*, **26**, 375–81.
- Merriman, R. J., and Peacor, D. R., 1999, Very low-grade metapelites: mineralogy, microfabrics and measuring reaction progress, in *Low-grade metamorphism* (eds. M. Frey and D. Robinson), 10–61, Blackwell Scientific, Oxford.
- Middleton, A. P., 1987, Technological investigation of the coatings on some 'haematite-coated' pottery from southern England, *Archaeometry*, **29**, 250–61.
- Muller, F., Drits, V., Plançon, A., and Robert, J. L., 2000, Structural transformation of 2 : 1 dioctahedral layer silicates during dehydroxylation–rehydroxylation reactions, *Clays and Clay Minerals*, **48**, 572–85.
- Nagasawa, K., and Ohkochi, N., 1988, X-ray studies on dehydration and rehydration of expandable clay minerals, *Thermochemica Acta*, **135**, 285–90.
- Peacor, D. R., 1992, Diagenesis and low-grade metamorphism of shales and slates, in *Minerals and reactions at the atomic scale: transmission electron microscopy* (ed. P. R. Buseck), 335–80, Reviews in Mineralogy 27, Mineralogical Society of America, Washington, DC.
- Pérez-Arategui, J., Molera, J., Larrea, A., Pradell, T., Vendrell-Sanz, M., Borgia, I., Brunetti, B. G., Cariati, F., Fermo, P., Mellini, M., Sgamellotti, A., and Viti, C., 2000, Lustre pottery from the 13th to the 16th century: a nanostructured thin metallic film, *Journal of the American Ceramic Society*, **84**, 442–6.
- Pérez Arrondo, C. L., 1987, El fenómeno megalítico en la margen derecha del Ebro: La Rioja. Estado de la cuestión y principales problemas, in *El megalitismo en la Península Ibérica*, 159–80, Vid, Madrid.
- Riccardi, M. P., Messiga, B., and Duminuco, P., 1999, An approach to the dynamics of clay firing, *Applied Clay Science*, **15**, 393–409.
- Rice, P. M., 1987, *Pottery analysis, a source book*, The University of Chicago Press, Chicago.
- Schomburg, J., 1991, Thermal reactions of the clay minerals: their significance as 'archaeological thermometers' in ancient potteries, *Applied Clay Science*, **6**, 215–20.

- Shoval, S., Beck, P., Kirsch, Y., Levy, P., Gaft, M., and Yadin, E., 1991, Rehydroxylation of clay minerals and hydration in ancient pottery from the 'land of Geshur', *Journal of Thermal Analysis*, **37**, 1579–92.
- Tazaki, K., and Fyfe, W. S., 1989, Growth of clay minerals in natural and synthetic glasses, *Clays and Clay Minerals*, **37**, 348–54.
- Tite, M. S., 1992, The impact of electron microscopy on ceramic studies, *Proceedings of the British Academy*, **77**, 111–31.
- Tite, M. S., and Maniatis, Y., 1975, Examination of ancient pottery using scanning electron microscope, *Nature*, **257**, 122–3.
- Tite, M. S., Freestone, I., Mason, R., Molera, J., Vendrell-Sanz, M., and Wood, N., 1998, Lead glazes in antiquity—methods of production and reasons for use, *Archaeometry*, **40**, 241–60.
- Veblen, D. R., Guthrie, G. D., Jr, Livi, K. J. T., and Reynolds, R. C., 1990, High-resolution transmission electron microscopy and electron diffraction of mixed-layer illite/smectite: experimental results, *Clays and Clay Minerals*, **38**, 1–13.
- Velde, B., and Druc, I. C., 1999, *Archaeological ceramic materials: origin and utilization*, Springer-Verlag, Berlin.
- Worden, R. H., Champness, P. E., and Droop, G. T. R., 1987, Transmission electron microscopy of the pyrometamorphic breakdown of phengite and chlorite, *Mineralogical Magazine*, **51**, 107–21.